Supplementary Information (SI)

for

Oxidation Mechanism of Phenols by Copper(II)-halide Complexes

Lan Yang, Rin Ito, Hideki Sugimoto, Yuma Morimoto, and Shinobu Itoh*

Department of Molecular Chemistry, Division of Applied Chemistry, Graduate School of Engineering, Osaka University, 2-1 Yamada-oka, Suita, Osaka 565-0871

E-mail: shinobu@chem.eng.osaka-u.ac.jp (S. Itoh)

Experimental

1. General. The reagents and solvents used in this study, except the ligand and the copper complexes, were commercial products of the highest available purity and used as received without further purification,[1] unless otherwise noted. The copper(II)-halide complexes $\mathbf{1}^{\mathbf{F}}$, $\mathbf{1}^{\mathbf{Cl}}$, $\mathbf{1}^{\mathbf{Br}}$, $\mathbf{1}^{\mathbf{I}}$, $\mathbf{2}^{\mathbf{Cl}}$, and $\mathbf{2}^{\mathbf{Br}}$ were prepared according to the reported procedures.[2-4] Ligand TMG_3tren was prepared according to the reported method.[5] All reactions were carried out under N_2 atmosphere using standard Schlenk technique or a glovebox (Miwa DB0-1KP or KK-011-AS, KOREA KIYON product, $[O_2]<1$ ppm). UV-visible spectra were taken on a Jasco V-570 or a Hewlett Packard 8453 photo diode array spectrophotometer equipped with a Unisoku thermostated cryostat cell holder USP-203. ^{1}H-NMR spectra were recorded on a JEOL JNM-ECS400 or a JEOL ECS400 spectrometer. Electrospray ionization mass spectra (ESI-MS) measurements were performed on a microTOF II focus (Bruker Daltonics). Matrix-assisted laser desorption/ionization time-of-flight (MALDI-TOF) mass spectra was taken on a JEOL JMS-S3000. Electron paramagnetic resonance (EPR) spectra were measured on a BRUKER EMX-micro continuous-wave X-band spectrometer, and simulated with the SpinCount program.[6]

2. Kinetic Analysis. Kinetic measurements for the reaction of copper(II) halide complexes $\mathbf{1}^{\mathbf{X}}$ with phenols $\mathbf{P}^{\mathbf{X}}$ were performed using a Hewlett Packard 8453 photo diode array spectrophotometer equipped with a Unisoku thermostated cryostat cell holder USP-203 (a desired temperature can be fixed within ± 0.5°C) in CH_3CN. Typically, the reaction of $\mathbf{1}^{\mathbf{Br}}$ with 2,4,6-tri-*tert*-butylphenol $\mathbf{P}^{\mathbf{t\!Bu}}$ was initiated by adding a substrate solution into a CH_3CN solution of $\mathbf{1}^{\mathbf{Br}}$ (0.25 mM) with use of a micro syringe at 0 °C. The reactions were monitored by following the decrease of absorption band at 410 nm due to $\mathbf{1}^{\mathbf{Br}}$, and the pseudo-first-order-rate constants (k_{obs}) of the reactions were obtained from the plot of $\ln(\Delta A)$ against the reaction time (t).

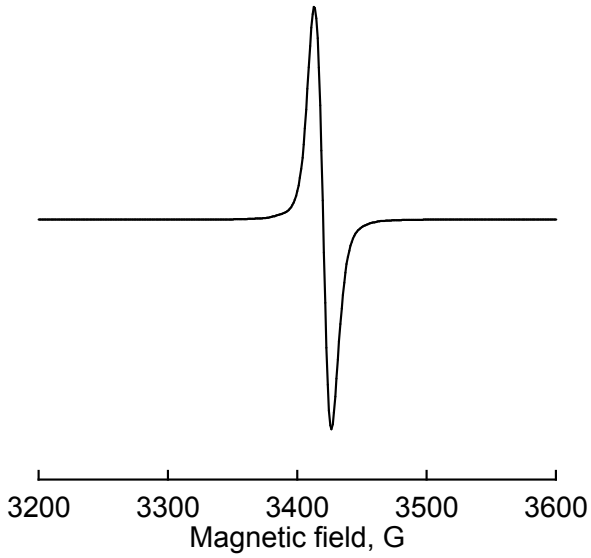

Fig. S1 X-band EPR spectra of the post reaction solutions showing the existence of phenoxyl radical ($\mathbf{P^{tBu}}$•) at g = 2.0041 in CH_2Cl_2 at 104 K. For the reaction of $\mathbf{1^{Br}}$ with $\mathbf{P^{tBu}}$H.

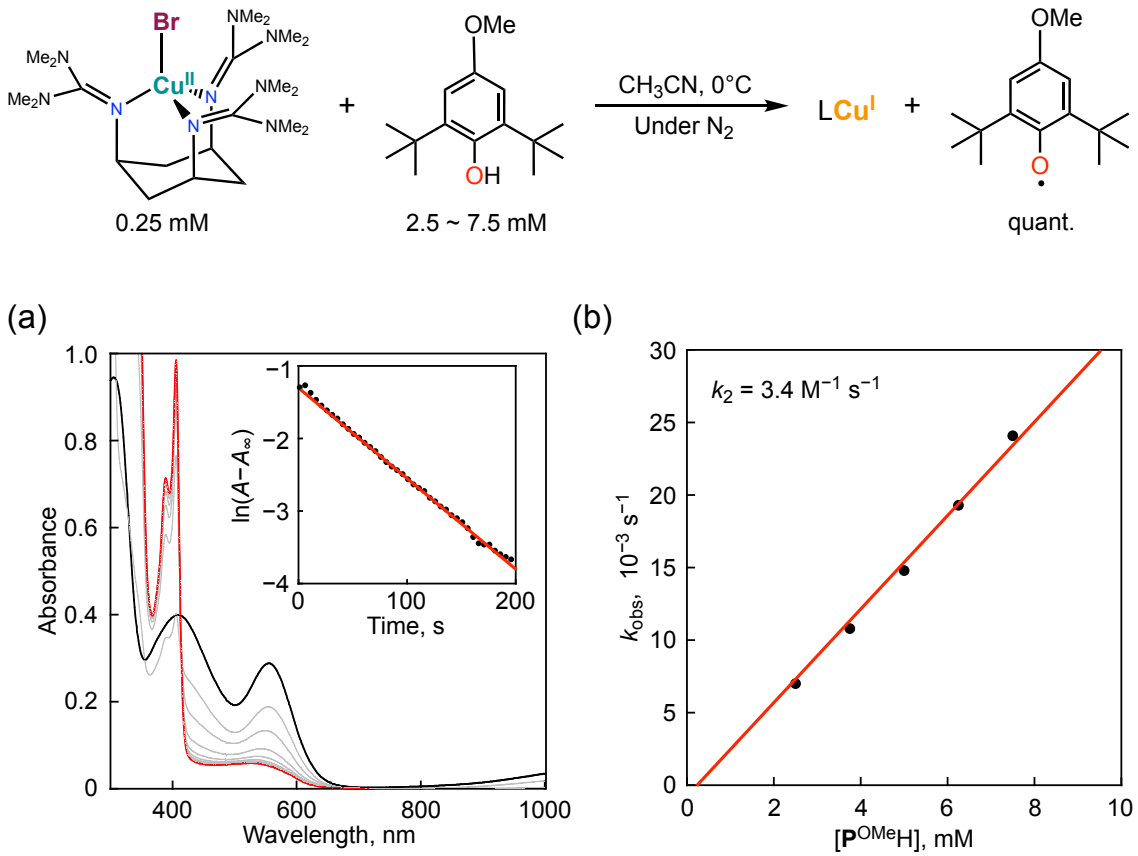

Fig. S2 (a) UV-vis spectral change for the reaction of $\mathbf{1}^{\mathbf{Br}}$ (0.25 mM) with 4-OMe-2,6-di-*tert*-butylphenol ($\mathbf{P}^{\mathbf{OMe}}$H, 5.0 mM) in CH_3CN at 0°C. Inset: Pseudo first-order plots based on the absorption change at 560 nm. (b) Plot of k_{obs} vs. [$\mathbf{P}^{\mathbf{OMe}}$H].

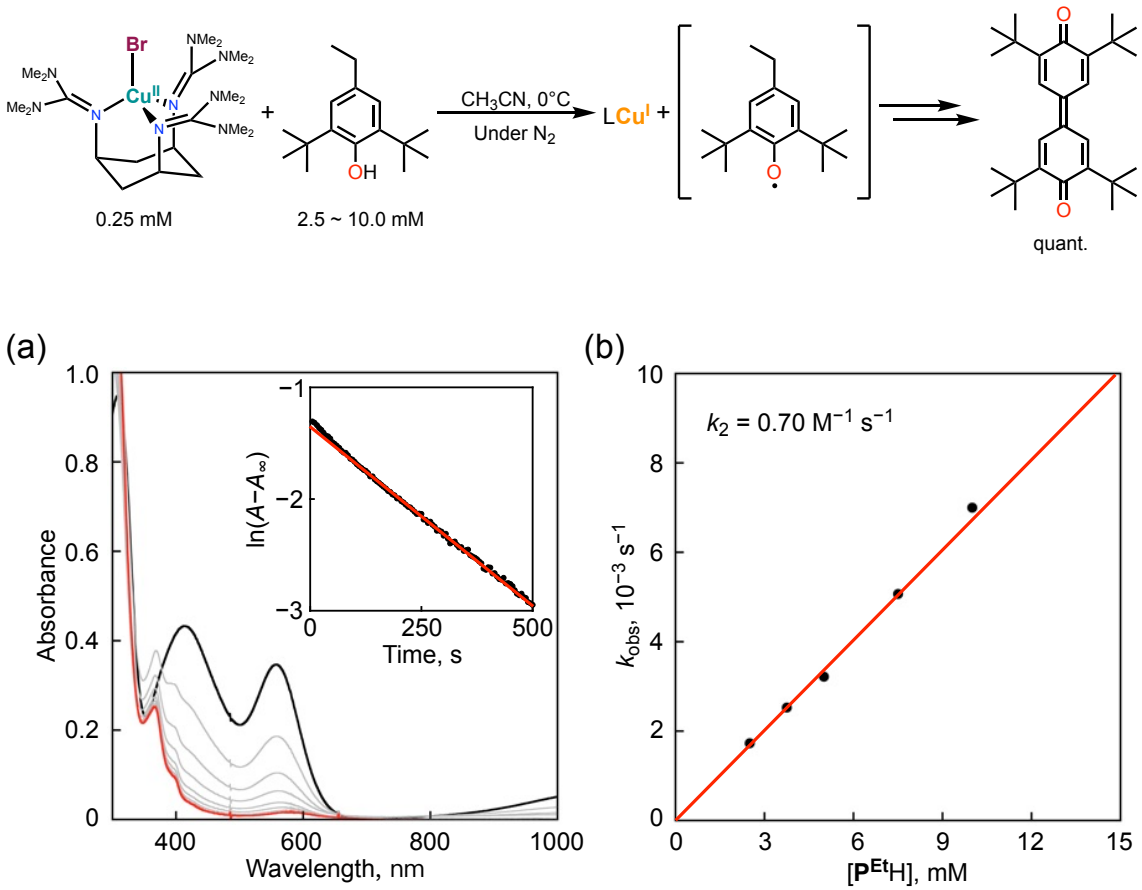

Fig. S3 (a) UV-vis spectral changes for the reaction of $\mathbf{1}^{\mathbf{Br}}$ (0.25 mM) with 4-ethyl-2,6-di-*tert*-butylphenol ($\mathbf{P}^{\mathbf{Et}}$**H,** 5.0 mM) in CH_3CN at 0°C. Inset: Pseudo first-order plots based on the absorption change at 560 nm. (b) Plot of k_{obs} vs. [$\mathbf{P}^{\mathbf{Et}}$H].

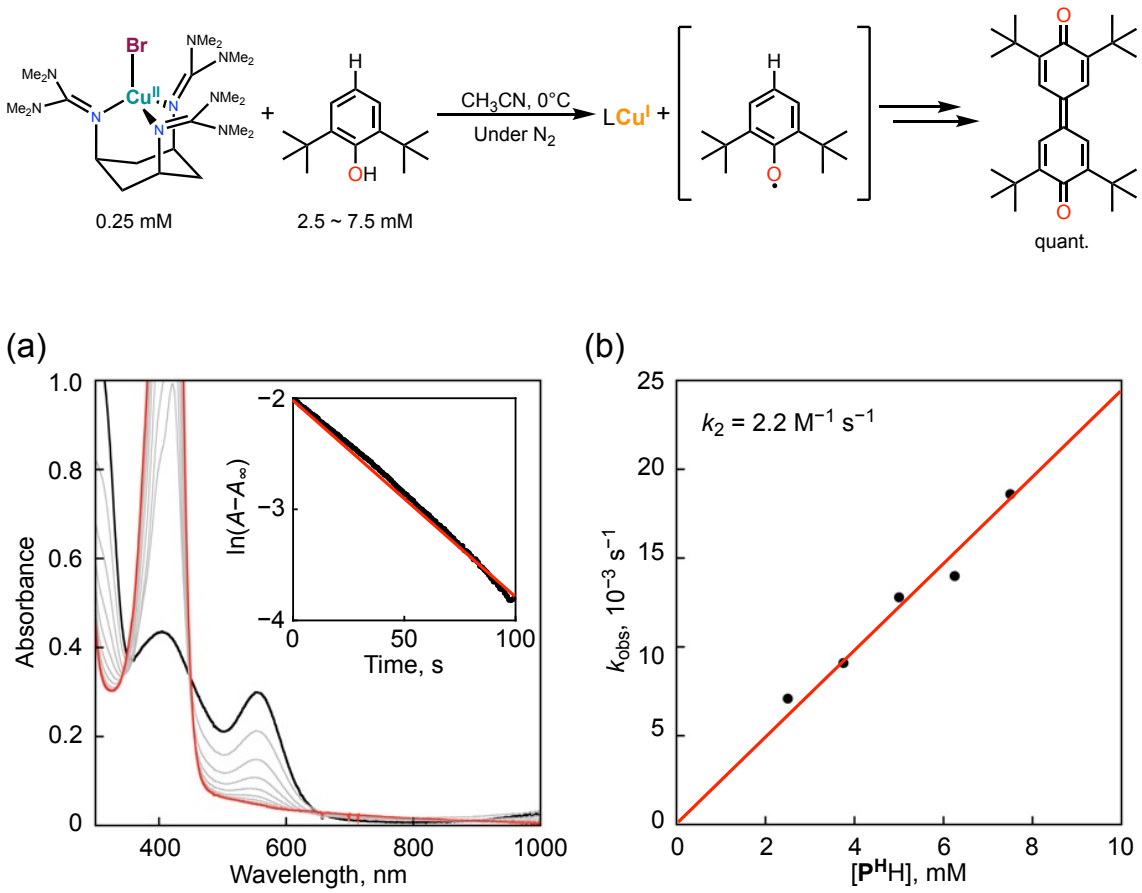

Fig. S4 (a) UV-vis spectral changes for the reaction of $\mathbf{1}^{\mathbf{Br}}$ (0.25 mM) with 2,6-di-*tert*-butylphenol ($\mathbf{P}^{\mathbf{H}}$H, 7.5 mM) in CH_3CN at 0°C. Inset: Pseudo first-order plots based on the absorption change at 560 nm. (b) Plot of k_{obs} vs. [$\mathbf{P}^{\mathbf{H}}$H].

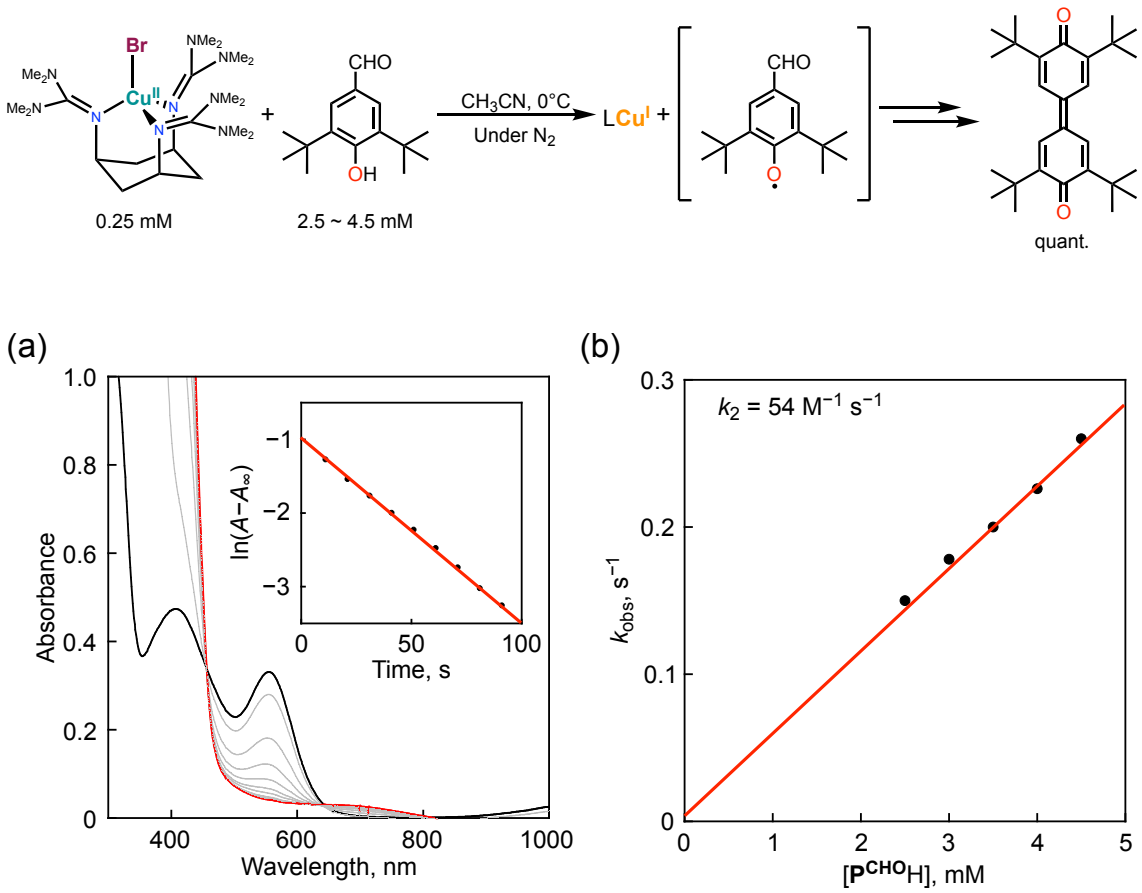

Fig. S5 (a) UV-vis spectral changes for the reaction of $\mathbf{1}^{\mathbf{Br}}$ (0.25 mM) with 4-formyl-2,6-di-*tert*-butylphenol ($\mathbf{P}^{\mathbf{CHO}}$H, 4.5 mM) in CH_3CN at 0°C. Inset: Pseudo first-order plots based on the absorption change at 560 nm. (b) Plot of k_{obs} vs. [$\mathbf{P}^{\mathbf{CHO}}$H].

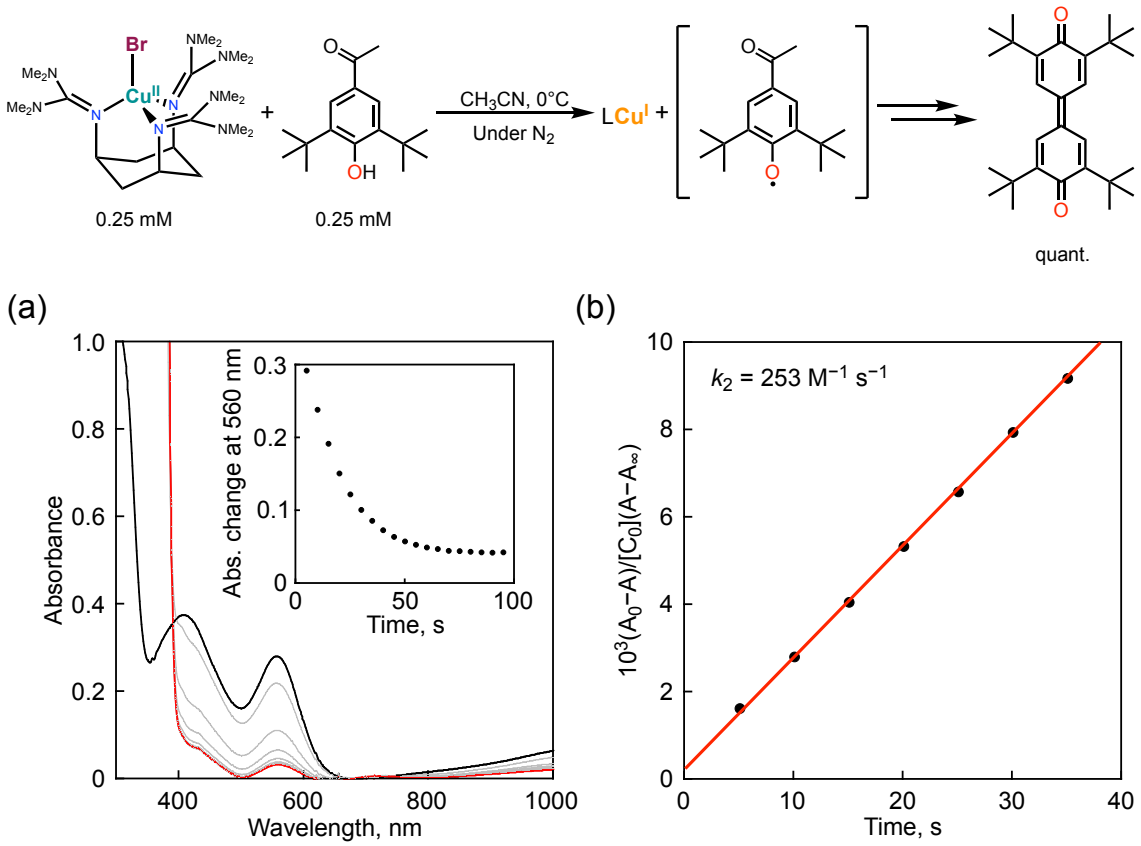

Fig. S6 (a) UV-vis spectral changes for the reaction of $\mathbf{1}^{\mathbf{Br}}$ (0.25 mM) with 4-COMe-2,6-di-*tert*-butylphenol ($\mathbf{P}^{\mathbf{COMe}}$H, 0.25 mM) in CH_3CN at 0°C. Inset: Absorption change at 560 nm. (b) Second-order plot based on the absorption change at 560 nm.

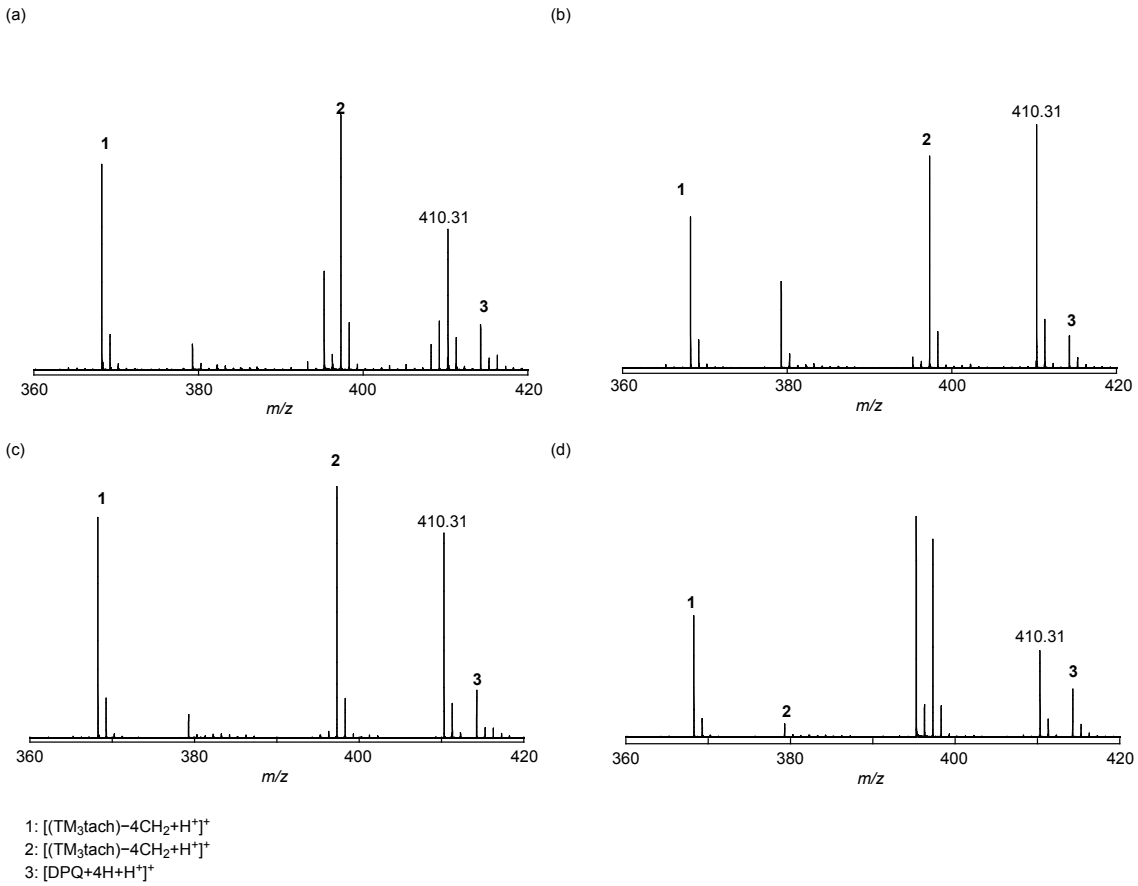

Fig. S7 MALDI-TOF mass spectra of the post reaction solutions showing the formation of 3,3',5,5'-tetra-*tert*-butyl-[1,1'-bi(cyclohexylidene)]-2,2',5,5'-tetraene-4,4'- dione+2H]$^+$ (*m/z* = 410.31) in the reactions of $\mathbf{1}^{\mathbf{Br}}$ and $\mathbf{P}^{\mathbf{Y}}$H 4-Y-2,6-di-*tert*-butylphenol; (a) Y = Et, (b) Y = H, (c) Y = CHO, and (d) Y = COMe.

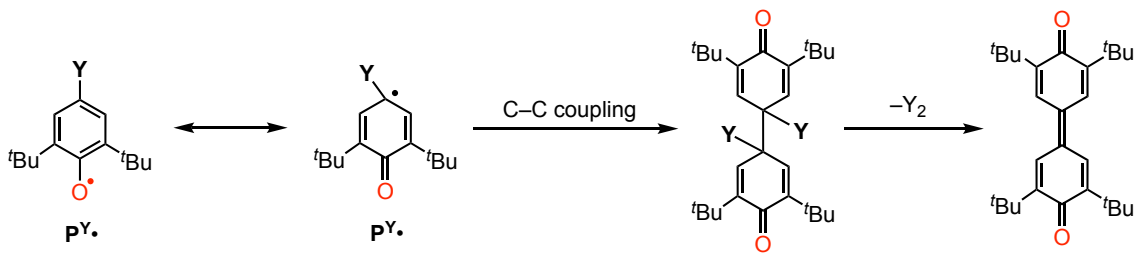

Scheme S1 Formation of 3,3',5,5'-tetra-*tert*-butyl-[1,1'-bi(cyclohexylidene)]-2,2',5,5'-tetraene-4,4'-dione by the C–C coupling reaction of $\mathbf{P}^{\mathbf{Y}}$•.

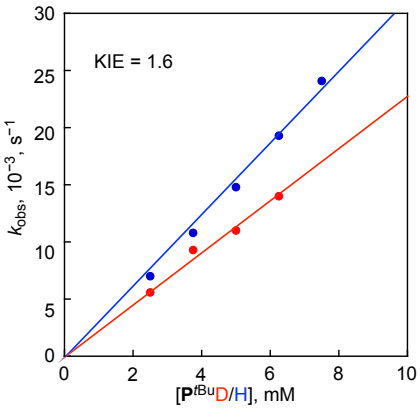

Fig. S8 Plots of k_{obs} against phenol concentration for the reaction between **1**^{Br} with **P**^{OMe}H (blue) and **P**^{OMe}D (red).

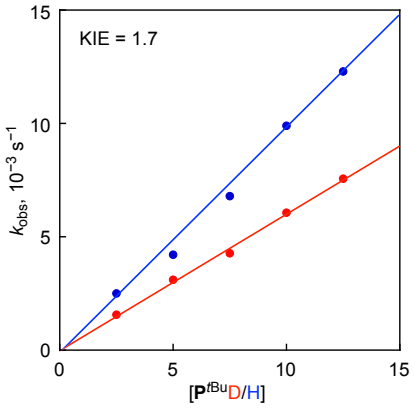

Fig. S9 Plots of k_{obs} against phenol concentration for the reaction between **1**^{Br} with **P**$^{t\mathrm{Bu}}$H (blue) and **P**$^{t\mathrm{Bu}}$D (red).

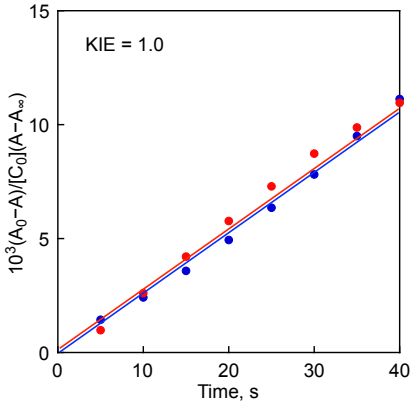

Fig. S10 Second-order plot for the reaction between $\mathbf{1}^{\mathbf{Br}}$ with $\mathbf{P}^{\mathbf{COMe}}$H (blue) and $\mathbf{P}^{\mathbf{COMe}}$D (red).

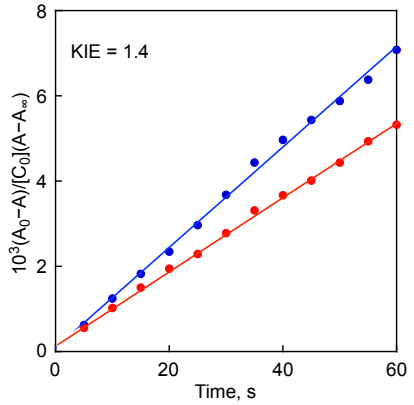

Fig. S11 Second-order rate constant plot for the reaction between $\mathbf{1}^{\mathbf{F}}$ with $\mathbf{P}^{\mathbf{COMe}}$H (blue) and $\mathbf{P}^{\mathbf{COMe}}$D (red).

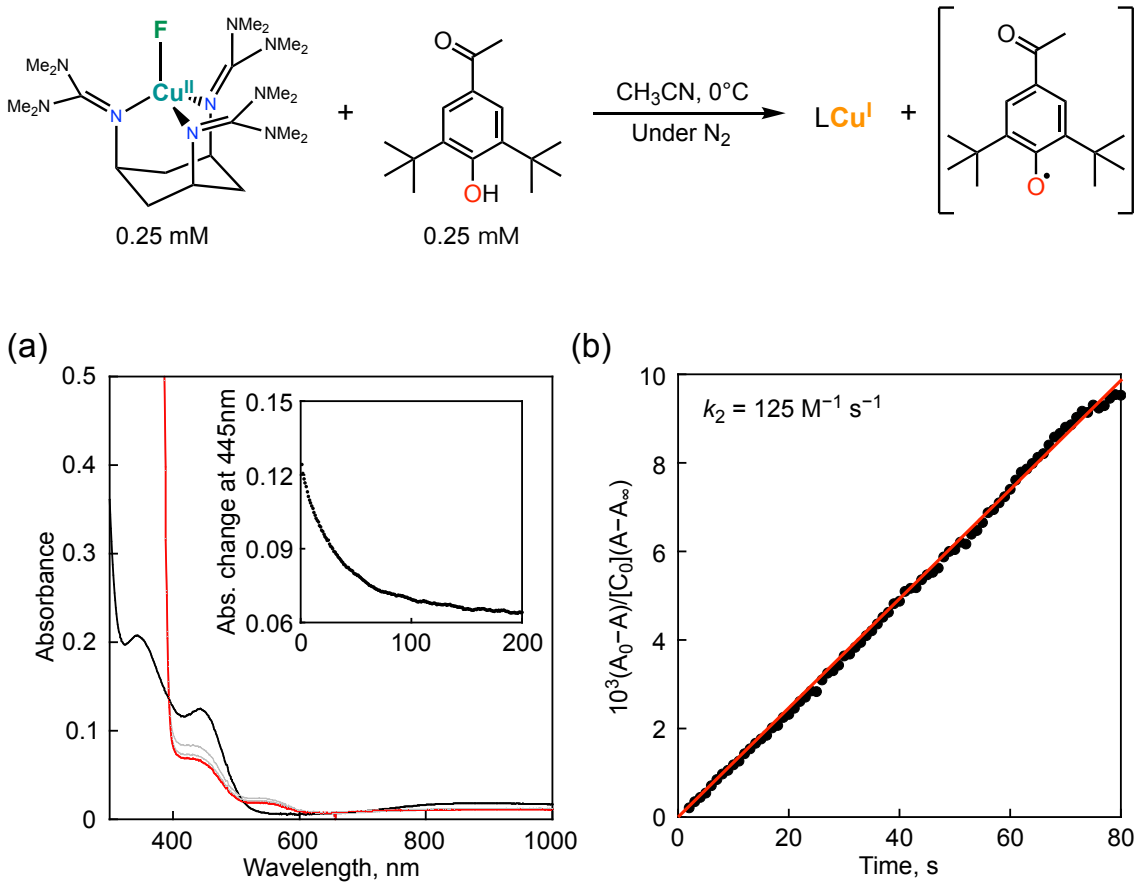

Fig. S12 (a) UV-vis spectral changes for the reaction of $\mathbf{1}^{\mathbf{F}}$ (0.25 mM) with 4-COMe-2,6-di-*tert*-butylphenol ($\mathbf{P}^{\mathbf{COMe}}$H, 0.25 mM) in CH_3CN at 0°C. Inset: Absorption change at 445 nm. (b) Second-order plot based on the absorption change at 445 nm.

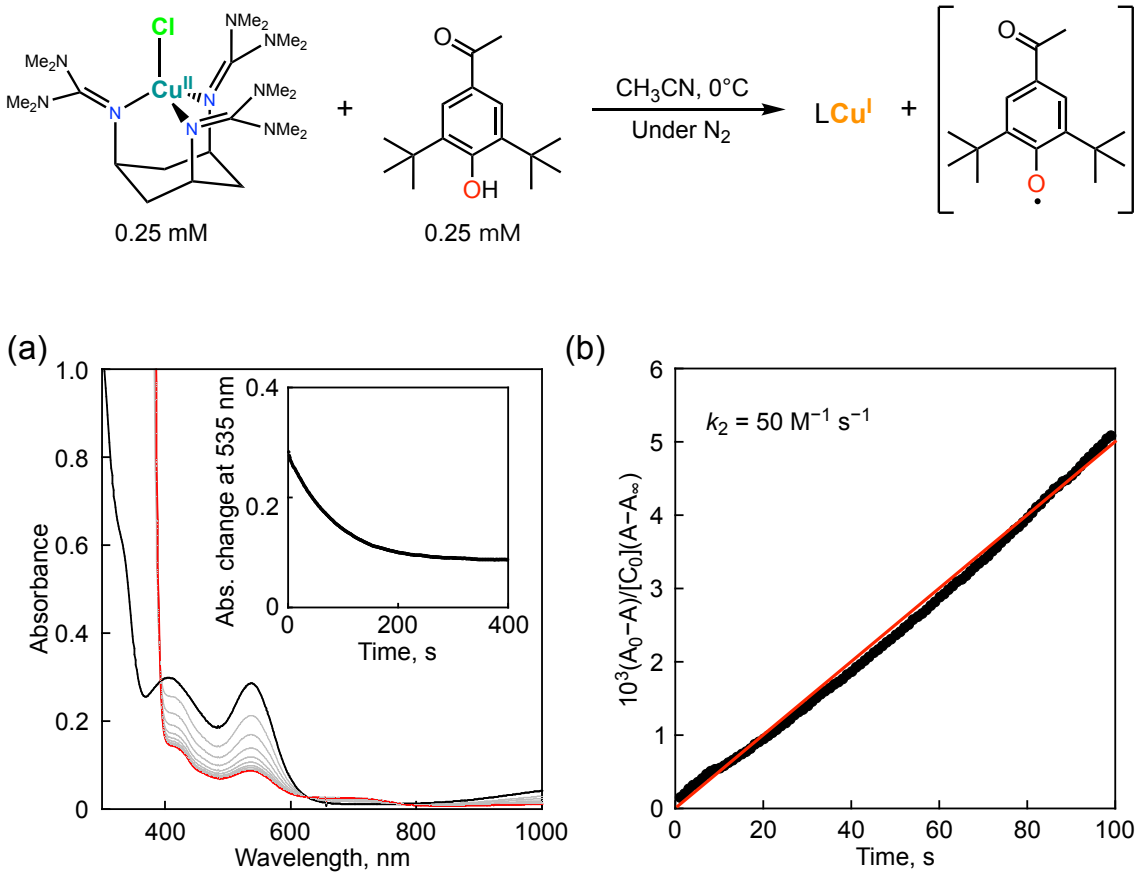

Fig. S13 (a) UV-vis spectral changes for the reaction of $\mathbf{1}^{\mathbf{Cl}}$ (0.25 mM) with 4-COMe-2,6-di-*tert*-butylphenol ($\mathbf{P}^{\mathbf{COMe}}$H, 0.25 mM) in CH_3CN at 0°C. Inset: Absorption change at 535 nm. (b) Second-order plot based on the absorption change at 535 nm.

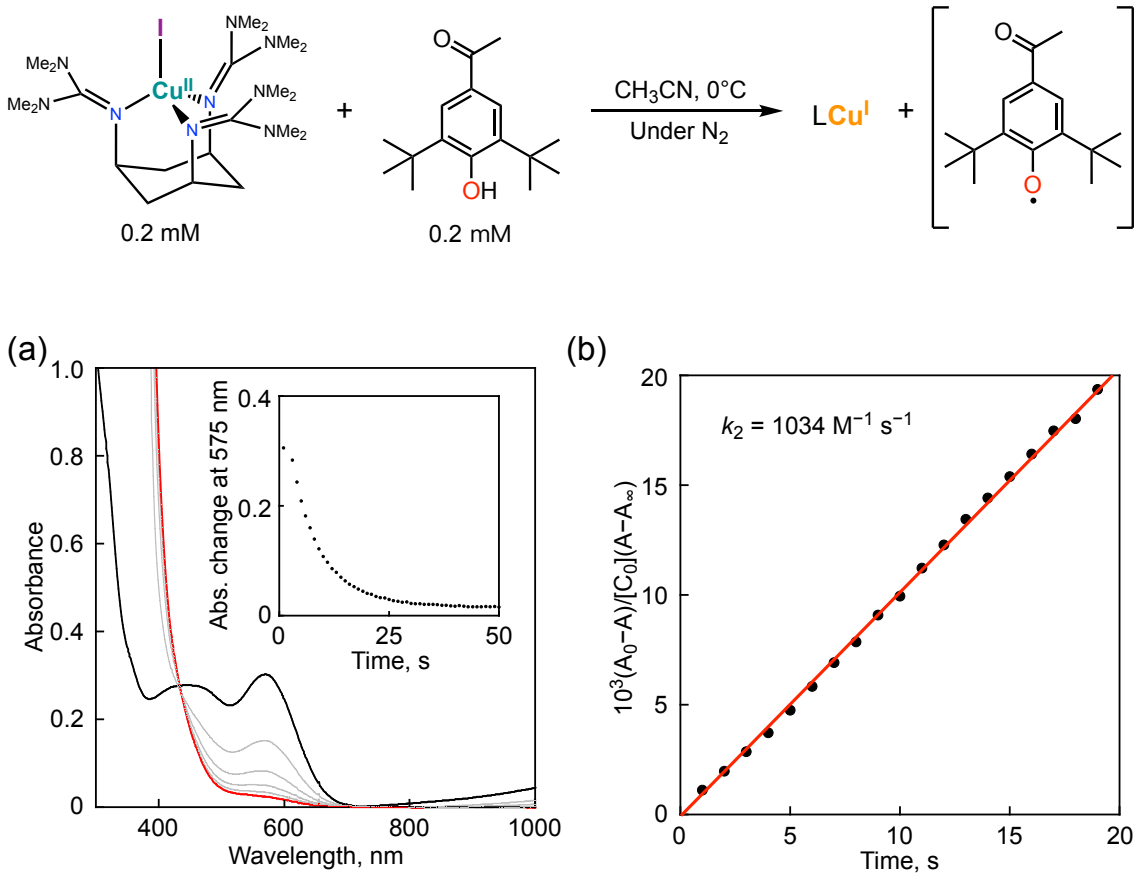

Fig. S14 (a) UV-vis spectral change for the reaction of $\mathbf{1}^{\mathbf{I}}$ (0.2 mM) with 4-COMe-2,6-di-*tert*-butylphenol ($\mathbf{P}^{\mathbf{COMe}}$H, 0.2 mM) in CH_3CN at 0°C. Inset: Absorption change based on absorbance at 575 nm. (b) Second-order plot based on the absorption change at 575 nm.

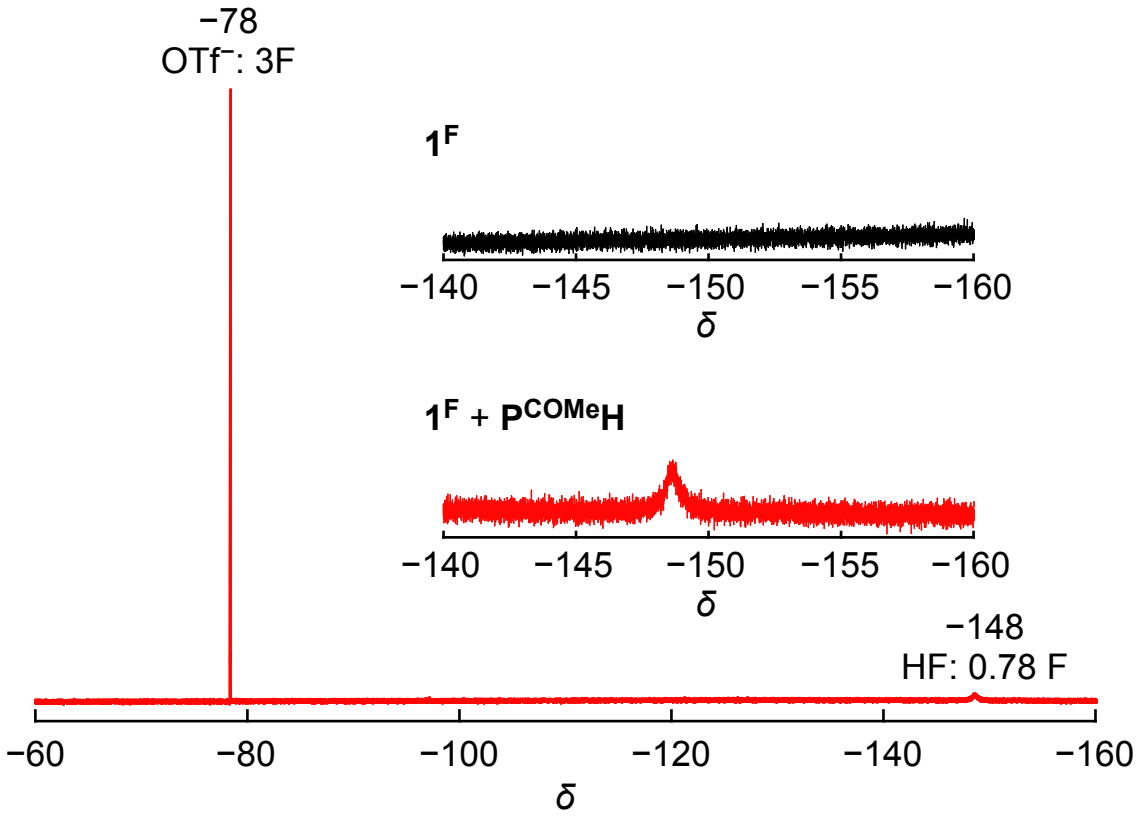

Fig. S15 ^{19}F NMR spectra of a post reaction solution of $\mathbf{1^F}$ and $\mathbf{P^{COMe}H}$ in CH_3CN. The yield of HF was determined by the integral ratio between OTf^- and HF.

1 *Purification of Laboratory Chemicals*, ed. by W. L. F. Armarego, Elsevier Science, **2017**.

2 Y. Lan, Y. Morimoto, I. Shimizu, H. Sugimoto, S. Itoh, *Inorg. Chem.* **2023**, *62*, 10539.

3 V. Raab, J. Kipke, O. Burghaus, J. Sundermeyer, *Inorg. Chem.* **2001**, *40*, 6964.

4 K. W. Kröckert, F. Garg, J. Heck, M. V. Heinz, J. Lange, R. Schmidt, A. Hoffmann, S. Herres-Pawlis, *Dalton Trans.* **2024**.

5 H. Wittmann, V. Raab, A. Schorm, J. Plackmeyer, J. Sundermeyer, *Eur. J. Inorg. Chem.* **2001**, *2001*, 1937.

6 D. T. Petasis, M. P. Hendrich, in *Electron Paramagnetic Resonance Investigations of Biological Systems by Using Spin Labels, Spin Probes, and Intrinsic Metal Ions, Pt A*, ed. by P. Z. Qin, K. Warncke, **2015**, Vol. 563, pp. 171.